ENVIRONMENTAL RESEARCH
LETTERS

LETTER • **OPEN ACCESS**

Radiocarbon as a tracer of the fossil fraction of regional carbon monoxide emissions

To cite this article: Liam Blyth *et al* 2024 *Environ. Res. Lett.* **19** 114073

IOP Publishing Environ. Res. Lett. 19 (2024) 114073 https://doi.org/10.1088/1748-9326/ad8248

ENVIRONMENTAL RESEARCH
LETTERS

OPEN ACCESS

RECEIVED
7 December 2023

REVISED
20 September 2024

ACCEPTED FOR PUBLICATION
2 October 2024

PUBLISHED
17 October 2024

LETTER

Radiocarbon as a tracer of the fossil fraction of regional carbon monoxide emissions

Liam Blyth[1,4,*], **Heather Graven**[1], **Alistair J Manning**[2] **and Peter Levy**[3]

[1] Department of Physics, Imperial College London, London SW7 2AZ, United Kingdom
[2] UK Met Office, Exeter EX1 3PB, United Kingdom
[3] Centre for Ecology and Hydrology, Bush Estate, Penicuik, Midlothian EH26 0QB, United Kingdom
[4] Science and Solutions for a Changing Planet DTP, Imperial College London, London SW7 2BX, United Kingdom
[*] Author to whom any correspondence should be addressed.

E-mail: liam.blyth20@imperial.ac.uk

Keywords: regional, carbon monoxide, radiocarbon, fossil fraction, modelling

Supplementary material for this article is available online

Abstract

Carbon monoxide (CO) is an atmospheric pollutant with a positive net warming effect on the climate. The magnitude of CO sources and the fraction of fossil vs biogenic sources are still uncertain and vary across emissions inventories. Measurements of radiocarbon (^{14}C) in CO could potentially be used to investigate the sources of CO on a regional scale because fossil sources lack ^{14}C and reduce the ^{14}C/C ratio (Δ^{14}C) of atmospheric CO more than biogenic sources. We use regional Lagrangian model simulations to investigate the utility of Δ^{14}CO measurements for estimating the fossil fraction of CO emissions and evaluating bottom-up emissions estimates (United Kingdom Greenhouse Gas, UKGHG, and TNO Copernicus Atmosphere Monitoring Service, TNO) in London, UK. Due to the high Δ^{14}CO in atmospheric CO from cosmogenic production, both fossil and biogenic CO emissions cause large reductions in Δ^{14}CO regionally, with larger reductions for fossil than biogenic CO per ppb added. There is a strong seasonal variation in Δ^{14}CO in background air and in the sensitivity of Δ^{14}CO to fossil and biogenic emissions of CO. In the UK, the CO emissions estimate from TNO has a higher fraction from fossil fuels than UKGHG (72% vs 67%). This results in larger simulated decreases in Δ^{14}C per ppb CO for TNO emissions. The simulated differences between UKGHG and TNO are likely to be easily detectable by current measurement precision, suggesting that Δ^{14}CO measurements could be an effective tool to understand regional CO sources and assess bottom-up emissions estimates.

1. Introduction

Carbon monoxide (CO) is a trace atmospheric gas which negatively impacts upon human health and indirectly contributes to climate change through its role in atmospheric chemistry. Removal of atmospheric CO is dominated by reaction with the hydroxyl radical (OH). CO has an atmospheric lifetime of ≈1–2 months, although this varies in different parts of the atmosphere (Holloway *et al* 2000). Although the direct radiative forcing effect of CO is negligible (Sinha and Toumi 1996), it accounts for 40% of the removal of OH, which impacts other species removed by OH (Lelieveld *et al* 2016). Since OH is a sink for methane, an increase in CO concentration leads to a longer atmospheric lifetime for methane, increasing its forcing effect. This radiative effect of CO was estimated to be ≈0.2 W^{-2} as calculated in the 5th IPCC assessment in 2013 (Myhre *et al* 2014).

Over the last 100 years, industrialisation led to a rise in CO emissions due to the incomplete combustion of fossil fuels and biomass, as well as an increase in chemical sources from oxidation of CH_4 (Duncan *et al* 2007). Some economies have regulated emissions in recent decades for health reasons. To reduce emissions, these countries introduced catalytic converters in cars and shifted from coal and wood-powered heating to gas-fired boilers. These trends caused CO emissions to first increase in Europe and North America in the 20th century, then decline in the 21st century

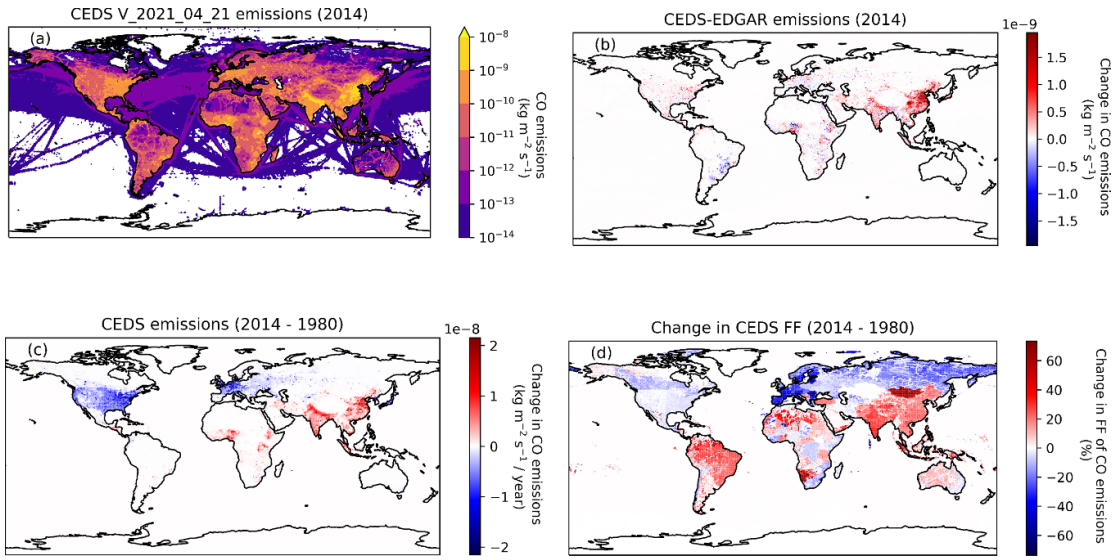

Figure 1. (a) CO emissions in 2014 from CEDS V_2021_04_21 (henceforth known as CEDS) (Hoesly *et al* 2018), (b) difference between CO emissions in CEDS and EDGAR version 6.1 in 2014 (c) difference in CO emissions in CEDS between 1980 and 2014 (d) difference in fossil fraction of CO emissions in CEDS between 1980 and 2014.

(Hoesly *et al* 2018). In these regions, a clear downward trend in atmospheric CO concentrations has been observed since the late 1990s, with a substantial decrease in the most extreme high CO events (figure 1) (Lowry *et al* 2016, Elguindi *et al* 2020). Along with a decrease in emissions, there has been a decrease in the fossil fraction of emissions as fossil fuel sources of CO have been mitigated more than biogenic sources. While the decrease in CO emissions in highly developed countries has stalled in recent years as many of the largest systematic and technological changes have already occurred, more work could still be done to further eliminate the remaining CO sources.

In regions that are in the process of industrialisation, such as in Asia and Africa, CO emissions and regional CO concentrations have risen over the past few decades and may continue to rise (figure 1). Observed CO concentrations sometimes conflict with inversion techniques using bottom-up emissions estimates, which may also show strong differences between different estimates (figure 1(b)), indicating that bottom-up approaches may not sufficiently quantify CO emissions. For example, observations by Zheng *et al* (2018) indicated that emissions from East China over 2005–2016 decreased by ≈2% yr^{-1}, in contrast to the increasing trends in emissions estimated by global inventories. This suggests that emissions controls may not be properly accounted for in bottom-up approaches.

Here, we explore how CO source attribution could be possible using ^{14}C, a radioactive isotope of carbon produced naturally in the atmosphere. The half-life of ^{14}C (5700 years) is significantly less than the age of fossil fuel sources (coal, gas). As a result, CO produced from fossil fuel burning will be devoid of ^{14}CO, as the ^{14}C that was present when the fuel source formed has decayed away. In contrast, CO produced from biogenic sources will have ^{14}C/C (Δ^{14}C, Δ including correction for mass dependent fractionation as defined in Stuiver and Polach 1977) ratios similar to atmospheric CO_2.

Δ^{14}C measurements have been widely used to partition fossil fuel and biogenic sources of CO_2 (Graven *et al* 2018) and aerosols (Al-Naiema *et al* 2018), but few previous studies have applied ^{14}CO measurements to examine regional CO sources (Klouda *et al* 1986, Moriizumi *et al* 2004). Klouda and Connolly (1995) used this method in Albuquerque, USA in the winter of 1989/90. They found that motor vehicles dominated emissions, but residential wood combustion increased in the winter. Similarly, Sakugawa and Kaplan (1997) conducted ^{14}CO measurements in Los Angeles, USA, and found that CO measured was predominantly of motor vehicle origin but that wood-burning was significant in winter.

Other measurements of ^{14}C in CO have been made to study CO loss by atmospheric OH rather than CO sources, and have typically been reported as molar density in units of molecules cm^{-3} rather than Δ^{14}C (Jöckel and Brenninkmeijer 2002). Compared to CO_2 and aerosols, Δ^{14}C of CO in background air is much higher (Brenninkmeijer *et al* 2022). Background values for Δ^{14}C vary significantly over the globe because the main source of ^{14}CO from cosmogenic production is focused in the high latitude upper troposphere and stratosphere (Poluianov *et al* 2016). This causes high Δ^{14}C in CO at surface levels at high latitudes, which varies seasonally due to the seasonal variation in stratosphere-troposphere exchange

(Quay *et al* 2000). Cosmogenic ^{14}CO production is modulated by the solar cycle, so background Δ^{14}CO also varies with solar activity. The high background Δ^{14}CO (2000‰–6000‰ estimated at Mace Head, Ireland) means that fossil (−1000‰) and biogenic (10‰–115‰ estimated for 2018) CO sources have a large difference in Δ^{14}C signature from background Δ^{14}CO, such that Δ^{14}CO will be highly sensitive to regional CO emissions.

Here we present the first simulations of Δ^{14}CO at a regional scale and use them to investigate the ability of Δ^{14}CO measurements to quantify the fossil fraction of CO emissions on regional scales. We use the Met Office's Numerical Atmospheric-dispersion Modelling Environment (NAME) to simulate CO and Δ^{14}CO at Imperial College London. We focus on Imperial College London (Saboya *et al* 2022) where we currently conduct atmospheric measurements, including CO concentrations, and where we plan to measure Δ^{14}C of CO in the future. From simulations based on different CO inventories and an idealised scenario, we simulate the effect of differences in the fossil fraction of CO emissions on Δ^{14}CO in London.

2. Methods

This section lays out the approach for simulating the CO concentration and Δ^{14}CO at Imperial College London for every hour in 2018. It will require an estimation of background CO and Δ^{14}CO, as well as an understanding of fuel sources and fossil fraction of different sectors in the emissions schemes being tested.

2.1. Mass-balance approach

This section lays out the mass balance approach used to simulate CO and Δ^{14}C. The mass-balance equation governing CO is:

$$C_m = C_{bg} + \sum_i C_i \quad (1)$$

where C_m represents the CO concentration simulated at our site of interest (Imperial College London), C_{bg} is the CO concentration at a background site (here, Mace Head, Ireland), and C_i is the simulated CO enhancement caused by emissions from sector i. Following previous studies of regional CO sources using Lagrangian models (Ding *et al* 2013, Andersen *et al* 2024), we assume that the effects of photochemical sources and sinks are negligible due to the short timescales (days) of air transport between background areas represented by Mace Head and the observation site in London.

The mass-balance equation governing ^{14}CO is:

$$\Delta_m C_m = \Delta_{bg} C_{bg} + \sum_i \Delta_i C_i. \quad (2)$$

Here, the additional terms Δ_m, Δ_{bg}, and Δ_i represent the Δ^{14}C of CO at our site of interest, at the background site, and in emissions from sector i, respectively. Compared to prior work with CO_2 and CH_4 where ^{14}C emissions from nuclear power plants have to be considered, it is unlikely that conditions amenable to the production of ^{14}CO are present in nuclear power plants and there are no indications of in-situ ^{14}CO production (Kunz 1985, Brenninkmeijer *et al* 2022). As with the CO mass balance, we assume photochemical sources and sinks have negligible effects on Δ_m for the short timescales of transport between background areas and London.

2.2. Background CO and Δ^{14}C

Very few ^{14}CO measurements are available for the last decade, so we construct an estimate of background Δ^{14}C at Mace Head (53.3° N, 9.9° W) in 2018 using historical data (Derwent *et al* 2020). For CO concentration, we use recent NOAA flask measurements at Mace Head, Ireland, for 2018. We find the monthly average CO mixing ratio and apply a sine function to calculate an estimated CO background for our simulations.

For ^{14}CO concentration, the background is estimated from measurements of ^{14}CO in Washington state, USA between 1991 and 1997 (Quay *et al* 2000). The measurement station in Washington State shares similarities with Mace Head, as it is on the west coast of a continent and receives predominantly clean air from over the ocean. It is also at a similar latitude as Mace Head (supplementary figure S1), meaning that background ^{14}CO values are expected to be similar. Since the cosmogenic ^{14}CO production is influenced by the solar cycle, a normalisation factor is applied to this estimate to transform into 2018 equivalent values. Average global production of ^{14}CO in 2018 was 1.964 molecules cm^{-2}, higher than the average between 1991 and 1997 (1.605 molecules cm^{-2}; calculated using the methodology presented in Poluianov *et al* 2016).

Firstly, all measurements from 1991 and 1997 are normalised to the production in 2018 using the following equation

$$C_{i,2018} = C_{i,t} * \frac{q_{2018}}{q_t} \quad (3)$$

where $C_{i,t}$ is the concentration in a given year, t, in a given month, i. q_{2018} is the estimated global production in 2018 (1.964 molecules cm^{-2}), q_i is the estimated global production in the year, t, and $C_{2018,t}$ is the normalised concentration, and so is $C_{i,t}$ normalised to 2018. This follows a similar process as Jöckel *et al* (2002), although we effectively normalise to an average solar production, and then 'unnormalise' to the solar production in 2018. We then calculate the average ^{14}CO for each month of 2018 and fit a sine function to generate our expected background. By combining our estimated CO and ^{14}CO we estimate Δ^{14}C at Mace Head with the assumption of δ^{13}C = −27.5‰ (Dasari *et al* 2022).

Table 1. Estimates of UK emissions and calculated fossil fraction for different emissions schemes using UKGHG, TNO and our constructed UKGHG_NT.

Emissions Scheme	Total UK emissions (ktonnes)	UK Fossil Fraction (%)
UKGHG	1875	67
TNO	1979	72
UKGHG_NT	1069	50

Table 2. Values of Δ^{14}C and fossil fraction used in the calculations and the fraction of UK emissions assigned to different sectors in the two schemes.

Sector	$\Delta^{14}C$ (‰)	Fossil Fraction (%)	UKGHG (%)	TNO(%)
Energy Production	−770	79	15.5	22.4
Domestic Combustion	−350	41	37.5	31.1
Industrial Combustion	−790	81	3.5	1.1
Industrial Processes	−1000	0	0	0
Offshore	−1000	0	0	0
Solvent	−20	12	0	0
Other Transport	−950	96	23.7	24.8
Road Transport	−950	96	14.1	17.1
Waste	−465	52	0.9	0.6
Nature	30	7	4.9	2.1

2.3. Regional anthropogenic sources

We use two different anthropogenic emissions estimates to simulate CO and Δ^{14}C at Imperial College London. These are the UK National Atmospheric Emissions Inventory with United Kingdom GHG time variability applied (UKGHG) and the TNO Copernicus Atmosphere Monitoring Service v5.3 (TNO) emissions inventory. They are similar in total UK CO emissions (1875 kilotonnes vs 1979 kilotonnes in 2018), however, the fuel source allocations and fossil fraction (FF, 67% vs 72%) vary (table 1).

UKGHG emissions are a UK-specific emissions estimates only covering the UK geographical area, whereas TNO emissions span Europe. For UKGHG simulations, the UKGHG's UK emissions have been nested in the TNO emissions for Europe.

We also consider a scenario (UKGHG_NT) in which the transport sector does not emit CO, which simulates the changes expected from a full transition to electric vehicles. We specify the emissions in this scenario by taking the UKGHG emissions embedded within TNO and removing all transport emissions.

To estimate the Δ^{14}C of each emission sector, we must first estimate Δ^{14}C for each fuel source. The UKGHG and TNO use the Selected Nomenclature for Air Pollution (SNAP) sectors for emissions maps, but contain no information on the fuel sources used; therefore, we use the fuel sources given for each sector in the National Atmospheric Emissions Inventory (NAEI) data for annual total emissions, which use Nomenclature for Reporting (NFR) sectors. For fossil fuels, Δ^{14}C is −1000‰. For biogenic sources, the age of the biomass burned must be considered. We use a simple one-box model with a specified turnover time together with the atmospheric history of Δ^{14}C in the Northern Hemisphere (Graven *et al* 2017). For older carbon sources, such as wood, the turnover time was assumed to be 50 years (personal correspondence with Forestry England), while for younger carbon sources, such as grasses, the turnover time was assumed to be 1 year, giving Δ^{14}C values of 115‰ and 10‰ in 2018, respectively. These values will be used for both natural and anthropogenic biomass burning. We map each NFR sector to a SNAP sector (supplementary table S1), such that we have the proportion of emissions in each SNAP sector derived from each fuel source (supplementary table S3). The Δ^{14}C for each SNAP sector is found by taking a weighted average of ^{14}C for each fuel source within that sector, weighting by CO emissions (table 2).

TNO include time variations that vary by sector (Guevara *et al* 2021), and UKGHG emissions are calculated by adding time variability to the otherwise temporally static NAEI (https://github.com/NERC-CEH/ukghg). The two main emissions sectors for CO are domestic combustion and transport emissions, and the yearly and daily/weekly variability in these two sectors can be seen in figure 2. Domestic combustion emissions are higher in the winter due to domestic heating. The UKGHG time variation is driven by activity and has a smooth variation throughout the year, whereas TNO variation is driven by the observed temperature and therefore has more irregular variation. Domestic combustion also shows a daily cycle, with a peak of emissions both early in the morning (10 am) and later in the evening (6 pm), with a slight decrease in the daytime (figure 2(c)). There is little yearly variability in traffic emissions (figure 2(b)), however, there is a significant daily cycle, with clear peaks in the morning and evening rush hours, and smaller transport emissions on the weekend.

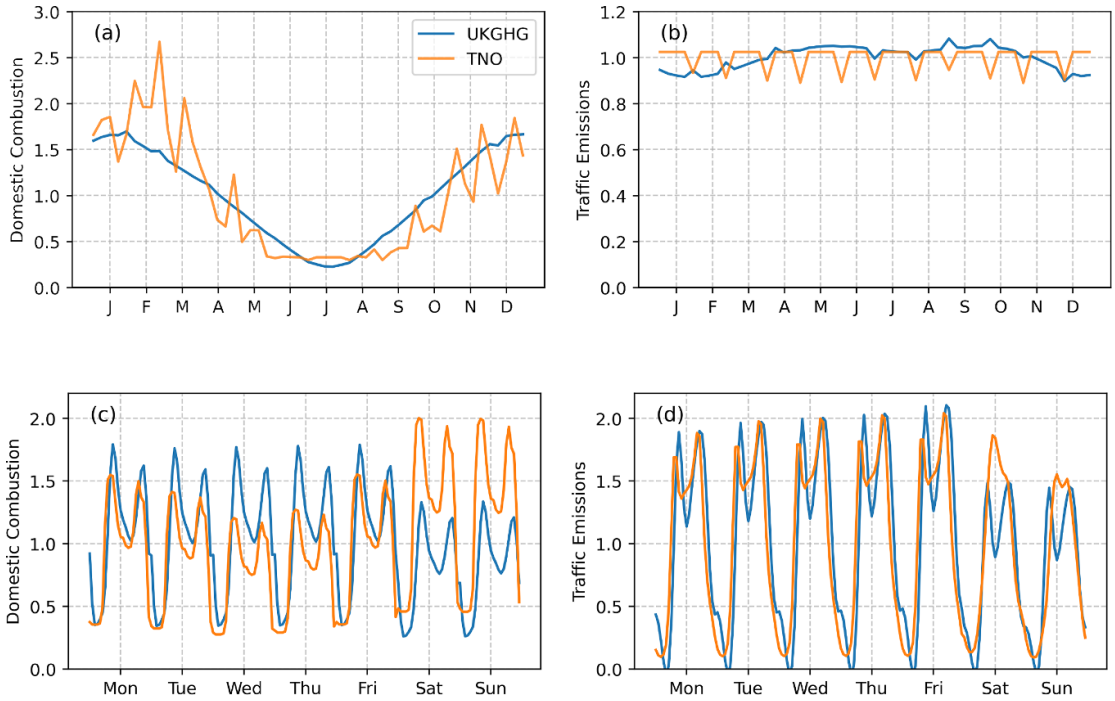

Figure 2. The normalised variability for the two main emissions sectors on different temporal scales for both UKGHG (blue) and TNO (orange) emissions in 2018. The yearly variation for domestic combustion in (a), and the yearly variation for traffic emissions in (b) shown as weekly averages. The weekly variation for domestic combustion can be seen in (c), and the weekly variation for traffic is seen in (d). In TNO, domestic combustion is calculated using atmospheric temperatures so there is no 'standard week'. Here, the first week of January was used.

2.4. NAME footprints

NAME was used to simulate CO at Imperial College London (≈26 m agl; 51.4999° N, 0.1749° W; Saboya *et al* 2022). NAME is a Lagrangian particle dispersion model driven by meteorological fields from a numerical weather prediction model, the Met-Office Unified Model (UM). Within the UK, UM resolution is at 1.5 km, outside it is 12 km. In the model, particles move in a three-dimensional grid with transport driven by the UM. There is also a random walk element to simulate the atmosphere's turbulence. No chemical production or destruction of CO was included.

The NAME model was run in backwards mode for a total of 30 days over the domain 97.9° W–39.38° E, and 10.73° N–79.06° N and footprints providing the sensitivity of an observation to emissions between 0 m and 40 m (surface) were calculated with a resolution of 0.356° × 0.234°. Footprints were calculated with hourly resolution for the first 24 h and the remaining 29 days were time-integrated. Footprints from the first 24 h with hourly resolution were multiplied by hourly emissions from UKGHG or TNO. The integrated footprint for the remaining 29 days enhancement was multiplied by the mean emissions for the month. These were then summed to produce the total simulated CO. Simulations were conducted for each emission sector and each hour in 2018.

3. Results

Simulated CO enhancements range from 2 to 225 ppb (daily 12:00–17:00 averages) and show a strong seasonality, with larger enhancements in winter (figure 3(a)) that arise for two reasons. First, there are generally lower boundary heights in winter than summer, so the air is not mixed as extensively. Since London is the largest polluter in the area, the emissions from London are more confined in the local area, leading to greater CO enhancements. Second, CO emissions are higher in winter due to the increased combustion associated with domestic heating (figure 2). These simulations match previous measurements in and around London which also show a strong seasonality (Hernández-Paniagua *et al* 2018).

The average daily CO enhancements for simulations with UKGHG and TNO emissions are nearly the same in their yearly median values (13.97 ppb vs 14.13 ppb), however, there are differences in medians for some months (figure 3(b)). CO enhancements from UKGHG_NT are lower (yearly median: 9.8ppb), as expected since traffic emissions that comprise 44% of UKGHG emissions were removed. This is more apparent in the summer when traffic emissions dominate the overall budget.

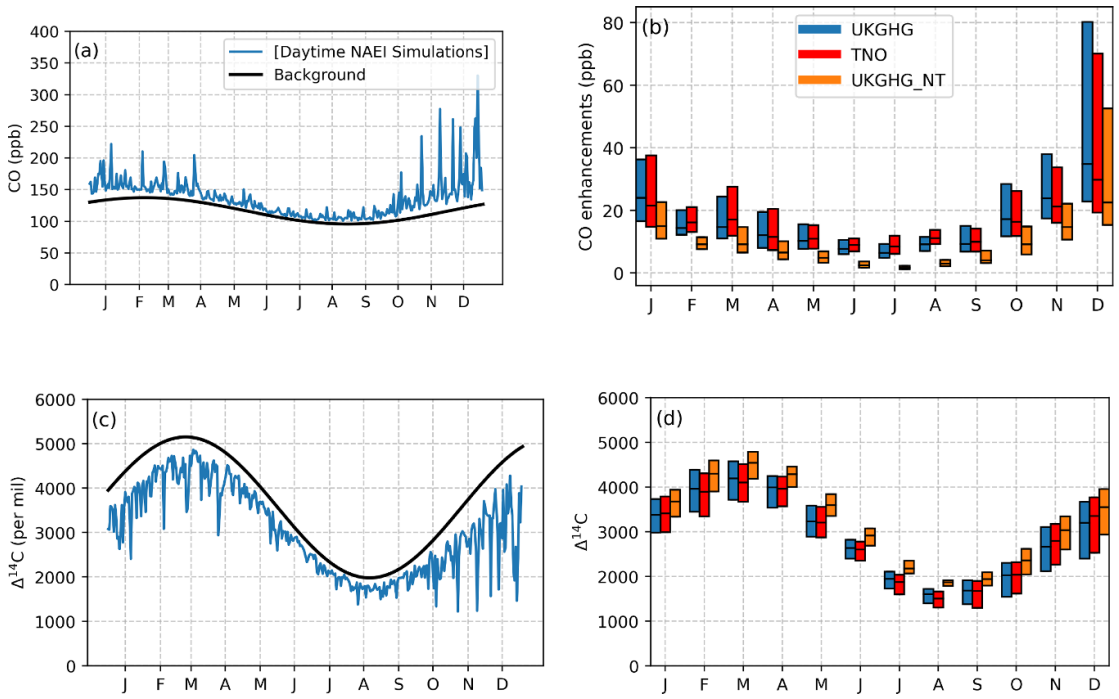

Figure 3. (a) Simulated CO enhancements at Imperial College London added to background CO concentrations from Mace Head, shown for afternoon hours (12:00–17:00 mean) in 2018 using UKGHG emissions. (b) Boxplots showing the 25th percentile, the median, and the 75th percentile of simulated CO enhancements for each month in 2018 from the three different emissions estimates. (c) Simulated Δ^{14}C at Imperial College London with estimated background for afternoon hours (1200–1700 mean) in 2018 using UKGHG emissions. (d) Boxplots showing the 25th percentile, the median, and the 75th percentile of simulated Δ^{14}C for each month in 2018 from the three different emissions estimates.

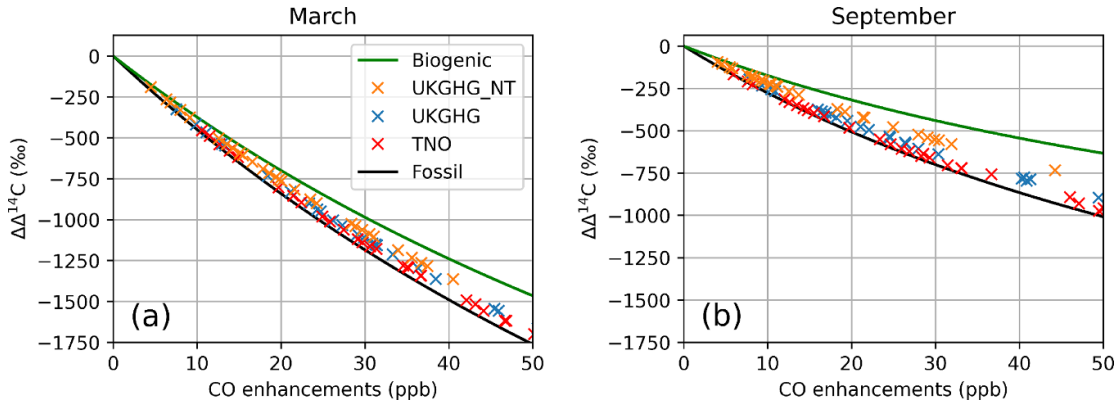

Figure 4. Simulated relationship between CO enhancements and $\Delta\Delta^{14}$C (daily mean) over two months (a) March and (b) September. All three emission schemes are shown, as well as ideal scenarios of purely fossil (black) and biogenic ($\Delta^{14}C = 30‰$) (green) CO emissions.

The difference between $\Delta^{14}C_m$ and $\Delta^{14}C_{bg}$ ($\Delta^{14}C_m$—$\Delta^{14}C_{bg}$, hereinafter referred to as $\Delta\Delta^{14}$C) varies with excess CO for the different simulations due to differences in fossil fraction (FF). Figure 4 shows the relationship between excess CO ($\sum_i C_i$) and $\Delta\Delta^{14}$C for March and September in the simulations, and when the additional CO is purely fossil (−1000‰) or purely biogenic (assuming 100‰). We chose these two months as they represent a large range of possible CO situations, one where background, Δ^{14}C and CO emissions are high (March), and one where all of these quantities are low (September). These curves use the monthly average ^{14}C as the background, and vary month by month due to the variation in the background Δ^{14}C of CO, which affects the sensitivity of Δ^{14}C to CO of different Δ^{14}C signatures. The difference between background Δ^{14}C in CO and fossil Δ^{14}C doubles between August and March. Background Δ^{14}C is also influenced by the solar cycle on multi-year timescales.

The three emissions scenarios follow distinct curves in figure 4 reflecting their different fossil fractions (table 1). UKGHG_NT has the lowest fossil fraction (yearly mean: 34%) and is nearest to the

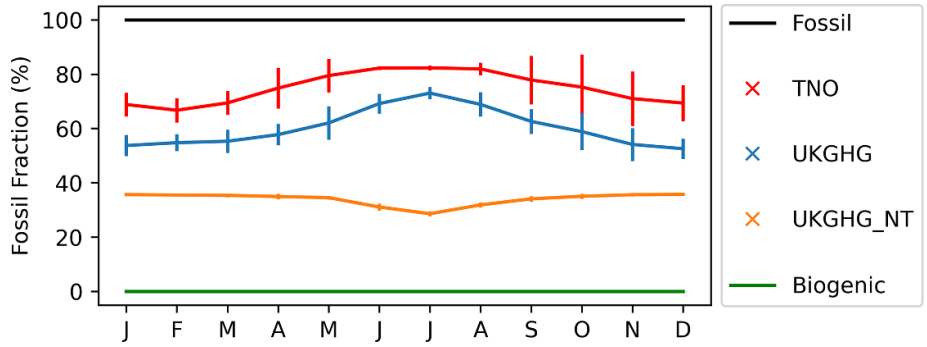

Figure 5. Derived mean monthly fossil fraction of CO at Imperial College London based on fitting simulated data from different emission schemes. Error bars show uncertainty in fits to idealised curves.

pure biogenic curve, while TNO has the highest fossil fraction (66%) and is nearest to the pure fossil curve. The UKGHG and TNO curves are closer to the pure fossil curve in summer months, when domestic combustion emissions are lower (figure 2).

There is some scatter in the Δ^{14}C-CO relationships for each scenario in figure 4, reflecting spatio-temporal variations in excess CO and the fossil fraction of CO in London. As an example of how Δ^{14}C and CO measurements could be interpreted for the monthly mean fossil fraction in excess CO, we compute idealized curves with different fossil fractions and find the best fit to the simulated data for each scenario. This best-fit fossil fractions can be seen in figure 5, with error bars representing 1σ uncertainties around the best-fit FF.

There is a lower fossil fraction in the winter than in the summer for UKGHG and TNO due to the increased domestic combustion emissions that use more biogenic fuel (figure 2(a)). In contrast, in summer, the bulk of emissions arise from transport, nearly all from fossil fuels. The fossil fraction in UKGHG_NT emissions remains relatively flat for the year, as the CO emissions in this regime are dominated by domestic combustion at all times with a fossil fraction of 34% (table 1).

There are significant differences between the derived fossil fractions for the different emission scenarios, compared to the uncertainty in the fits (≈5%), indicating Δ^{14}C measurements would help to refine CO source attribution in London. Uncertainties in Δ^{14}C and CO measurement are comparable to the scatter in each scenario in figure 4, suggesting that the uncertainties in derived fossil fraction would not be much larger than these estimated uncertainties. Considering the UKGHG_NT scenario, it appears that Δ^{14}C measurements would be able to track reductions in fossil fraction as the UK transitions to electric vehicles following bans on the sale of internal combustion and hybrid vehicles planned over the coming decade.

4. Potential methodology for exploiting ^{14}CO measurements to determine CO fossil fraction

The results of our simulations using different emissions schemes and the NAME model demonstrate a proof of concept to understand how ^{14}CO measurements could be applied to determine the fossil fraction of CO at Imperial College or at other locations. To apply this technique, the required measured parameters are:

- Measurements of CO mixing ratio (C_m) and Δ^{14}CO (Δ_m) at a measurement site
- Measurements of CO mixing ratio (C_{bg}) and Δ^{14}CO (Δ_{bg}) at a background location
- Measurement or estimation of Δ^{14}C of the biogenic source of CO in the region (Δ_{bio}).

These data could then be plotted as in figure 4, with $\Delta\Delta^{14}$C vs CO enhancements, and compared to idealised curves to find the average fossil fraction that best matches the data.

Alternatively, the fossil-derived CO (C_{ff}) can be calculated directly from an individual measurement following the mass balances from equations (1) and (2) using the equation (Turnbull *et al* 2006):

$$C_{ff} = \frac{(\Delta_m - \Delta_{bio})\,C_m - (\Delta_{bg} - \Delta_{bio})\,C_{bg}}{(\Delta_{ff} - \Delta_{bio})}. \quad (4)$$

And the fossil fraction of the CO enhancement can be calculated using the equation:

$$FF = C_{ff}/\left(C_m - C_{bg}\right). \quad (5)$$

By propagating errors (see supplementary material), we find the uncertainty on measured C_{ff} would be ∼10% on an individual measurement for typical scenarios at Imperial College. This assumes the uncertainty of CO mixing ratio is ±2 ppb, uncertainty of Δ_{bio} is ±250‰ and uncertainty of Δ^{14}CO

measurements to be ±125‰ (Petrenko *et al* 2021). Since the uncertainty in fossil fraction will be dominated by the uncertainty on the derived C_{ff}, uncertainty on calculated FF will also be ±10%, which should allow us to trace a wide range of possible CO emissions scenarios. For other locations where CO enhancements are much higher, the uncertainty would be lower.

Some applications should also consider chemical sources, such as the oxidation of CH_4 or VOCs (Dasari *et al* 2022), or sinks from CO oxidation, which we neglected. One way of accounting for chemical effects might be to combine $\Delta^{14}C$ with stable isotopic measurements of CO to enhance our understanding of the origin of excess CO.

5. Discussion and conclusions

We presented the first regional-scale simulations of ^{14}CO and showed that there are differences in $\Delta\Delta^{14}C$-excess CO relationships at Imperial College London driven by differences in the fossil fraction of CO emissions that should be detectable with current measurement precision. The capability of ^{14}CO measurements to identify fossil fraction is unique, as $^{13}C/^{12}C$ in CO from fossil fuels and biomass burning are similar (Vimont *et al* 2017).

Our results indicate that ^{14}CO measurements could be used to evaluate the fossil fraction of regional CO emissions and compared with bottom-up emission inventories, and to track trends in the fossil fraction of CO emissions over time. Evaluating and improving the source attribution of CO emissions would help to mitigate emissions and evaluate the effectiveness of mitigation policies, including the phaseout of internal combustion engines in the UK. Observations of seasonal changes in the fossil fraction of CO sources could also help to better understand CO sources.

A better understanding of CO sources could also benefit applications using CO measurements as a tracer for fossil fuel-derived CO_2 (Turnbull *et al* 2015). The use of CO as a tracer of fossil fuel-derived CO_2 assumes that fossil fuel combustion is the dominant source of CO in a region, an assumption that could be checked with measurements of $\Delta^{14}C$ in CO.

The sensitivity of $\Delta^{14}C$ to regional emissions will change year on year because the background $\Delta^{14}CO$ changes due to the solar cycle. For 2018, our background varies between 1978‰ and 5150‰, however, for a year with low solar activity we would expect this to be higher (≈2800‰–5550‰), whilst in years with high solar activity, this would be lower (≈1100‰–2250‰). Therefore, the sensitivity will be highest during solar minimum.

The application of $\Delta^{14}C$ measurements to attribute CO sources may be particularly useful in the regions where CO sources may be less well-known. Considering global emissions of CO (shown for two bottom-up estimates in figure 1), the highest emissions of CO in 2014 are in Asia and Africa, which also have the largest differences between bottom-up estimates and are among the places with the strongest growth in emissions since 1980. The technique would also be more effective there due to the stronger sources of CO and higher excess CO concentrations. In addition, there is less variation in $\Delta^{14}C$ of background CO in lower latitudes compared to higher latitudes, which could reduce the uncertainty in the derived fossil fraction.

Data availability statement

NAEI mapped emissions for 2018 can be found at: https://naei.energysecurity.gov.uk/data/maps/download-gridded-emissions whilst UKGHG time variations can be applied using R package at https://github.com/NERC-CEH/ukghg. Total yearly emissions allocated by fuel source can be found at: https://naei.beis.gov.uk/data/data-selector.

TNO_CAMSv5.3 are available to download directly from ECCAD website (https://eccad.aeris-data.fr). CAMS_TEMPO, the temporal variability applied to TNO_CAMSv5.3 emissions can be found at: https://eccad.sedoo.fr/#/metadata/506 (last accessed November 2023).

Estimated background CO and $\Delta^{14}C$, along with simulated CO and $\Delta^{14}CO$ for each emission scheme can be found in supplemental data in table S2. The mapping between NFR and SNAP sectors is found in supplemental data in table S1. The SNAP sector emissions, split into fuel sources, can be found in supplemental data in table S3.

All data that support the findings of this study are included within the article (and any supplementary files).

Acknowledgments

L B was supported by the Grantham Institute—Climate Change and the Environment and the Natural Environment Research Council [NE/S007415/1]. H G would like to acknowledge funding from the Natural Environment Research Council [NE/X001040/1], from a Royal Society Wolfson Fellowship [RSWF/FT/191013] and from Schmidt Sciences through the Fate, Emissions, and Transport of CH_4 (FETCH4) project. Analysis code was based on functions provided by Dr Hannah Chawner (previously of University of Bristol).

ORCID iDs

Liam Blyth https://orcid.org/0000-0002-2246-7838
Heather Graven https://orcid.org/0000-0003-3934-2502
Peter Levy https://orcid.org/0000-0002-8505-1901

References

Al-Naiema I M, Yoon S, Wang Y-Q, Zhang Y-X, Sheesley R J and Stone E A 2018 Source apportionment of fine particulate matter organic carbon in Shenzhen, China by chemical mass balance and radiocarbon methods *Environ. Pollut.* **240** 34–43

Andersen C, Ketzel M, Hertel O, Christensen J H and Brandt J 2024 The Danish Lagrangian Model (DALM): development of a new local-scale high-resolution air pollution model *Environ. Modelling Softw.* **176** 106010

Brenninkmeijer C A M, Gromov S S and Jöckel P 2022 Cosmogenic ^{14}CO for assessing the OH-based self-cleaning capacity of the troposphere *Radiocarbon* **64** 761–79

Dasari S, Andersson A, Popa M E, Röckmann T, Holmstrand H, Budhavant K and Rjan Gustafsson O 2022 Observational evidence of large contribution from primary sources for carbon monoxide in the South Asian outflow *Environ. Sci. Technol.* **56** 165–74

Derwent R, Parrish D, Simmonds P G, O'Doherty S J and Spain T G 2020 Seasonal cycles in baseline mixing ratios of a large number of trace gases at the Mace Head, Ireland atmospheric research station *Atmos. Environ.* **233** 117531

Ding A, Wang T and Fu C 2013 Transport characteristics and origins of carbon monoxide and ozone in Hong Kong, South China *J. Geophys. Res. Atmos.* **118** 9475–88

Duncan B N, Logan J A, Bey I, Megretskaia I A, Yantosca R M, Novelli P C, Jones N B and Rinsland C P 2007 Global budget of CO, 1988–1997: source estimates and validation with a global model *J. Geophys. Res. Atmos.* **112** 1988–97

Elguindi N *et al* 2020 Intercomparison of magnitudes and trends in anthropogenic surface emissions from bottom-up inventories, top-down estimates and emission scenarios *Earth's Future* **8** 1–20

Graven H *et al* 2017 Compiled records of carbon isotopes in atmospheric CO_2 for historical simulations in CMIP6 *Geosci. Model Dev.* **10** 4405–17

Graven H *et al* 2018 Assessing fossil fuel CO_2 emissions in California using atmospheric observations and models *Environ. Res. Lett.* **13** 065007

Guevara M, Jorba O, Tena C, Denier Van Der Gon H, Kuenen J, Elguindi N, Darras S, Granier C and Pérez García-Pando C 2021 Copernicus atmosphere monitoring service TEMPOral profiles (CAMS-TEMPO): global and European emission temporal profile maps for atmospheric chemistry modelling *Earth Syst. Sci. Data* **13** 367–404

Hernández-Paniagua I Y *et al* 2018 Diurnal, seasonal and annual trends in tropospheric CO in Southwest London during 2000–2015: wind sector analysis and comparisons with urban and remote sites *Atmos. Environ.* **177** 262–74

Hoesly R M *et al* 2018 Historical (1750–2014) anthropogenic emissions of reactive gases and aerosols from the Community Emissions Data System (CEDS) *Geosci. Model Dev.* **11** 369–408

Holloway T, Levy H II and Kasibhatla P 2000 Global distribution of carbon monoxide *J. Geophys. Res. Atmos.* **105** 12123–47

Jöckel P and Brenninkmeijer C A M 2002 The seasonal cycle of cosmogenic ^{14}CO at the surface level: a solar cycle adjusted, zonal-average climatology based on observations *J. Geophys. Res. Atmos.* **107** ACH 23–1–20

Jöckel P, Brenninkmeijer C A M, Lawrence M G, Jeuken A B M and van Velthoven P F J 2002 Evaluation of stratosphere-troposphere exchange and the hydroxyl radical distribution in three-dimensional global atmospheric models using observations of cosmogenic ^{14}CO *J. Geophys. Res* **107** 4446

Klouda G A and Connolly M V 1995 Radiocarbon (^{14}C) measurements to quantify sources of atmospheric carbon monoxide in urban air *Atmos. Environ.* **29** 3309–18

Klouda G A, Currie L A, Donahue D J, Jull A J T and Naylor M H 1986 Urban atmospheric ^{14}CO and $^{14}CH_4$ measurements by accelerator mass spectrometry *Radiocarbon* **28** 625–33

Kunz C 1985 Carbon-14 discharge at three light-water reactors *Health Phys.* **49** 25

Lelieveld J, Gromov S, Pozzer A and Taraborrelli D 2016 Global tropospheric hydroxyl distribution, budget and reactivity *Atmos. Chem. Phys.* **16** 12477–93

Lowry D *et al* 2016 Marked long-term decline in ambient CO mixing ratio in SE England, 1997–2014: evidence of policy success in improving air quality *Sci. Rep.* **6** 25661

Moriizumi J, Goto A and Iida T 2004 A new extraction technique for atmospheric ^{14}CO and its application *Nucl. Instrum. Methods Phys. Res.* B **223-224** 511–5

Myhre G *et al* 2014 Anthropogenic and natural radiative forcing *Climate Change 2013-The Physical Science Basis* pp 659–740

Petrenko V V, Smith A M, Crosier E M, Kazemi R, Place P, Colton A, Yang B, Hua Q and Murray L T 2021 An improved method for atmospheric ^{14}CO measurements *Atmos. Meas. Tech.* **14** 2055–63

Poluianov S V, Kovaltsov G A, Mishev A L and Usoskin I G 2016 Production of cosmogenic isotopes ^{7}Be, ^{10}Be, ^{14}C, ^{22}Na and ^{36}Cl in the atmosphere: altitudinal profiles of yield functions *J. Geophys. Res. Atmos.* **121** 8125–36

Quay P, King S, White D, Brockington M, Plotkin B, Gammon R, Gerst S and Stutsman J 2000 Atmospheric ^{14}CO: a tracer of OH concentration and mixing rates *J. Geophys. Res. Atmos.* **105** 15147–66

Saboya E, Zazzeri G, Graven H, Manning A J and Englund Michel S 2022 Continuous CH_4 and $\delta^{13}CH_4$ measurements in London demonstrate under-reported natural gas leakage *Atmos. Chem. Phys.* **22** 3595–613

Sakugawa H and Kaplan I R 1997 Radio and stable-isotope measurements of atmospheric carbon monoxide in Los Angeles *Geochem. J.* **31** 75–83

Sinha A and Toumi R 1996 A comparison of climate forcings due to chlorofluorocarbons and carbon monoxide *Geophys. Res. Lett.* **23** 65–68

Stuiver M and Polach H A 1977 Reporting of ^{14}C data *Radiocarbon* **19** 355–63

Turnbull J C *et al* 2015 Toward quantification and source sector identification of fossil fuel CO_2 emissions from an urban area: results from the INFLUX experiment *J. Geophys. Res.* **120** 292–312

Turnbull J C, Miller J B, Lehman S J, Tans P P, Sparks R J and Southon J 2006 Comparison of $^{14}CO_2$, CO and SF_6 as tracers for recently added fossil fuel CO_2 in the atmosphere and implications for biological CO_2 exchange *Geophys. Res. Lett.* **33** L01817

Vimont I J *et al* 2017 Carbon monoxide isotopic measurements in Indianapolis constrain urban source isotopic signatures and support mobile fossil fuel emissions as the dominant wintertime CO source *Elementa* **5** 1–17

Zheng B, Chevallier F, Ciais P, Yin Y, Deeter M N, Worden H M, Wang Y, Zhang Q and He K 2018 Rapid decline in carbon monoxide emissions and export from East Asia between years 2005 and 2016 *Environ. Res. Lett.* **13** 044007